The Space instrument SOVAP of the PICARD mission

C. Conscience[a], M. Meftah[b,*], A. Chevalier[a], S. Dewitte[a] and D. Crommelynck[a]

[a] RMIB, Avenue Circulaire, 3, 1180 Uccle, Belgique
[b] CNRS/INSU, LATMOS-IPSL, Université Versailles St-Quentin, Guyancourt, France

ABSTRACT

PICARD is a Satellite dedicated to the simultaneous measurement of the absolute total and spectral solar irradiance, the diameter and solar shape and the Sun's interior probed by helioseismology method. Its objectives are the study of the origin of the solar variability and the study of the relations between the Sun and the Earth's climate. PICARD was launched on June 15, 2010. The Satellite was placed into the heliosynchronous orbit of 735 km with inclination of 98.28 degrees. The payload consists in two absolute radiometers measuring the TSI (Total Solar Irradiance) and an imaging telescope to determine the solar diameter, the limb shape and asphericity. SOVAP (SOlar VAriability Picard) is an experiment developed by the Belgian STCE (Solar Terrestrial Center of Excellence) with a contribution of the CNRS (Centre National de la Recherche Scientifique) composed of an absolute radiometer provided by the RMIB (Royal Meteorological Institute of Belgium) to measure the TSI and a bolometer provided by the ROB (Royal Observatory of Belgium). The continuous observation of the solar irradiance at the highest possible precision and accuracy is an important objective of the Earth climate change. This requires: high quality metrology in the space environment. In this article, we describe the SOVAP instrument, its performances and uncertainties on the measurements of the TSI.

Keywords: Solar Astrometry, Total Solar Irradiance, Micro-satellite, Sun, Instrumentation, PICARD, SOVAP

1. INTRODUCTION

The solar mission PICARD will simultaneously measure several key parameters of the Sun [1]. These parameters are essential for the understanding of the physics of the Sun. One of these parameters is the Total Solar Irradiance (TSI). The TSI is a measure of the radiative output from the Sun. Its value and its long-term variability have a direct impact on the Earth's climate. The scientific objectives of the PICARD mission are described in details by [2]. Although sunspots have been observed since about 1610 showing periodic solar activity, the Solar Irradiance (SI) reduced to one A.U. (Astronomical Unit) is observed from space, only since 1978 and continuously since this date from space by using radiometers. The mean value of the TSI calculated on the RMIB composite from December 17, 1984 to December 24, 2008 is 1366.64 W/m^2 [8] with a standard deviation of 0.58 W/m^2, an absolute accuracy better than 1.36 W/m^2 (or 1000 ppm) and a resolution of 0.0136 W/m^2. The early space-borne measurements of TSI were suffering from a high level of noise and, more problematically, from poor absolute accuracy. With time, improvements in instrumentation allowed to converge towards the 1366.64 W/m^2 value for the TSI. The efforts were then concentrated on the long-term TSI stability of individual instruments. With the launch in 2003 of the TIM (Total Irradiance Monitor) on board SORCE (Solar Radiation and Climate Experiment), controversy on the TSI absolute value has been re-initiated. TIM has indeed measured a TSI value that is approximately 4.5 W/m^2 lower than the average measurement of the simultaneously flying radiometers. This triggered the interest of performing new TSI absolute measurements and more particularly, better quantification of the inherent uncertainties. Given that the scientific objectives require measurement as a function of solar activity, a very high stability of the SOVAP instrument on the whole duration of the mission, is mandatory. RMIB and CNRS has manufactured and tested a very high dimensional stability instrument using advanced technology. The RMIB TSI composite is shown in the Figure 1 and the different missions addressing the same scientific issues are listed in Table 1.

* Corresponding author
E-mail address: Mustapha.Meftah@latmos.ipsl.fr

2. THE MISSION CONSTRAINTS

The PICARD mission is operated during the rising phase of the solar cycle 24 allowing us to study the relationship between all the measurements simultaneously gathered, in particular between the diameter and the Total Solar Irradiance. The orbit is chosen to allow periods of Sun visibility as long as possible for the helioseismologic measurements (internal structure of the Sun) and to provide the best conditions for the instruments thermal stability. A SSO (Sun Synchronous Orbit) with an ascending node at 06h00, an altitude of 735 km and an inclination of 98.28 degree was selected. The duration of eclipses will not exceed 20 minutes with these orbit parameters, in particular in December. The mission lifetime is two years; however a longer mission is expected especially given the late start of cycle 24.

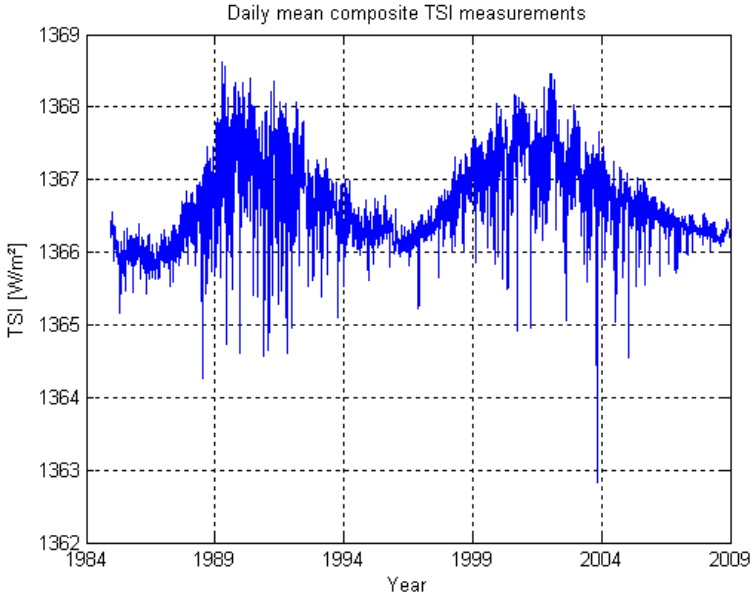

Figure 1. TSI composite from RMIB.

Table 1. Long term space born measurements.

Date	Instruments and flights	Authors and reference
1978-1993	HF/ERB on Nimbus 7	Hickey et al. [14] [15], Kyle et al. [16]
1980-1989	ACRIM1 on SMM	Willson & Hudson [17], Willson et al. [18]
1984-2003	ERBE on ERBS	Barkstrom [19], Lee et al. [20]
1985-1989	ERBE on NOAA 9	Barkstrom et al. [21]
1986-1987	ERBE on NOAA 10	Barkstrom et al. [21]
1991-2001	ACRIM2 on UARS	Willson & Mordvinov [22]
1992-1993	SOVA 1 (CR 11) on EURECA	Crommelynck et al. [23] [24]
1992-1993	SOVA 2 on EURECA	Romero et al. [25]
1996-?	DIARAD (CR 15)/VIRGO on SOHO	Dewitte et al. [10]
1996-?	PMO6/VIRGO on SOHO	Fröhlich et al. [26], Finsterle et al. [27]
2000-?	ACRIM3 on ACRIMSAT	Willson & Helizon [28]
2003-?	TIM on SORCE	Kopp et al. [29]
2010-?	DIARAD/SOVAP on PICARD	–
2010-?	PMO6/PREMOS on PICARD	–

3. THE SOVAP INSTRUMENT

SOVAP is a DIfferential Absolute RADiometer (DIARAD) developed at RMIB. The DIARAD type radiometers have been designed and developed by D. Crommelynck financed by the FRFCIM (Fonds de la Recherche Fondamentale Collective d'Initiative Ministérielle). They were the first side by side absolute cavity radiometers to be flown in space [9]. The SOVAP measurements will provide continuity for the measurements obtained from DIARAD/VIRGO since 1996 [10] and SOLCON (SOLar CONstant instrument) on the space shuttle in 1983, 1992, 1993, 1994, 1995, 1997, 1998, and 2003 [11]. TIM/SORCE is a side by side cavity radiometer independent from the DIARAD series launched in 2003. The comparison of DIARAD/VIRGO and TIM/SORCE, although with a difference of 4.5 W/m^2, has demonstrated a repeatability of 0.1 W/m^2 for this kind of design.

3.1 The SOVAP principle

SOVAP radiometric core is formed by two blackened cavities constructed side by side on a common heat sink. A heat flux transducer (sensor) is mounted between each cavity and the heat sink. The difference between the two balanced sensors outputs gives an instantaneous differential heat flux measurement, in which the common part of the thermal surrounding radiation seen by the two cavities is eliminated. By symmetrical construction, good insulation and proper selection of thermo-optical materials, thermal asymmetry is minimized. Both channels are equipped with a shutter in front of them, by which sunlight can be occulted (closed shutter) or allowed into (open shutter) the cavity. In the open shutter phase, solar radiative power flows into the cavity through a precision aperture and is absorbed. The cavity is cylindrical and is covered with diffuse black paint. Besides solar radiative power, electrical power can be dissipated by a resistor mounted in the cavity. During the design of the cavities, careful attention has been paid to obtain corresponding spatial locations and distributions for the solar and the electrical heating power flowing directly into the heat flux sensor. See Figure 2 for the main features of SOVAP. While SOVAP is a recurrent design, with gradual improvement in time, we added a Bolometric Oscillation Sensor (BOS) to increase the time resolution. BOS will measure the Solar Irradiance, the infrared flux of the Earth and the albedo flux with a smaller sampling period of ten seconds. The relative BOS measurements at ten seconds sampling will be calibrated by the absolute DIARAD measurements every three minutes. A cross section of DIARAD cavity is shown in Figure 3. The field of view is 1.192^o.

The design of D. Crommelynck's instrument [3], is the same as the one flown on VIRGO/SOHO [4] and performs the comparison of the two channels thermal fields by differential heat flux measurement with respect to a common thermal reference [5]. Yet, the instrument is slightly different by the use of titanium precision apertures and another shutter thermal design. Those apertures have been measured in three different Laboratories: The JPL (Jet Propulsion Laboratory), the NPL (National Physical Laboratory) [6] and the NIST (National Institute of Standards and Technologies) [7]. We introduced SSM (Second Surface Mirror) on the shutters (Sun side) to reduce their temperature. The DIARAD cavity principle is shown in Figure 14.

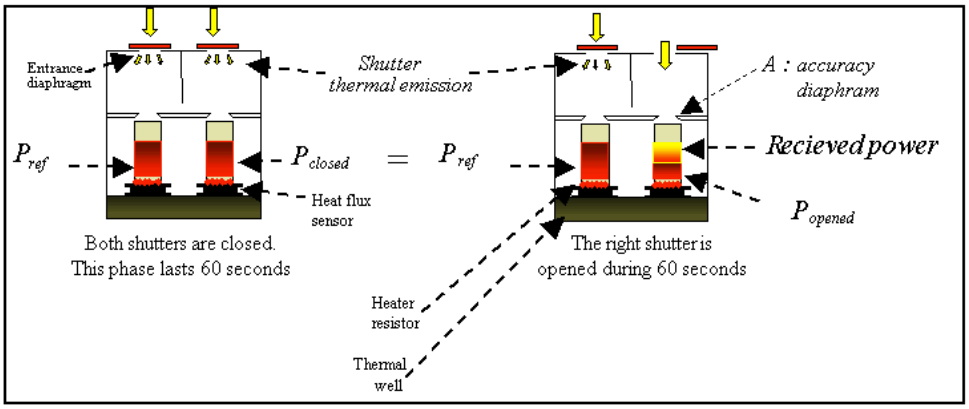

Figure 2. Main features of SOVAP - during the closed and open phases.

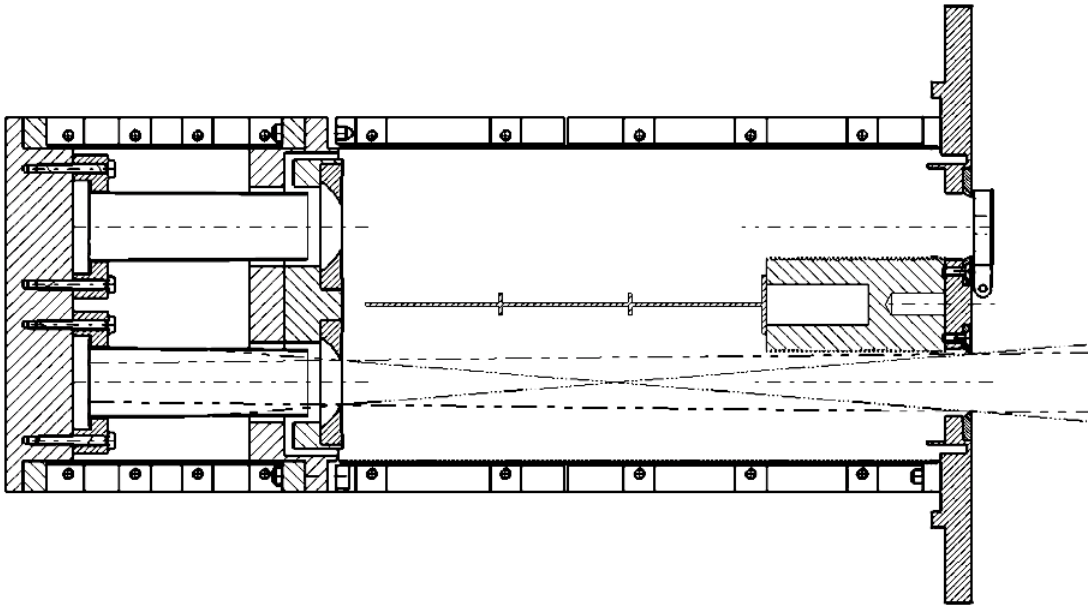

Figure 3. Cross section of DIARAD/SOVAP cavity.

3.2 The SOVAP interface characteristics

The PICARD payload is operated by global on-board electronics named the PGCU (PICARD Gestion Charge Utile or PICARD Payload Management Unit). Table 2 summarizes the main characteristics of SOVAP instrument. The precision aperture mirror is shaped as a concave spherical reflective surface, focalized in the center of the front aperture to minimize backscattering.

Table 2. SOVAP main characteristics.

Volume	347 (d) x 180 (w) x 268 (h) mm^3
Weight	9.4 kg
Field of view	1.192^o
Power Consumption	10.1 W nominal and 11.0 W maximum
Data Rate	348 Kbits per day

3.3 The mechanisms and the radiometric states

SOVAP uses mobile mechanisms such as a system to open and close the shutter. In the nominal measurement sequence, a constant electrical power is fed into one cavity, the reference cavity, while its shutter remains closed. The electrical power in the other cavity, the measurement cavity, is regulated continuously; while its shutter sequentially open and close (both open and closed states take 90 seconds). When the instrument is pointed to the Sun, the power equilibrium is maintained by the electrical power in the measurement cavity which drops proportionally to the absorbed solar power. The instrument design allows 15 different combinations of servo side and status of the servo-system and of the shutters called radiometric states. This unique feature of the DIARAD design allows different tests to be performed in space to verify the coherence of the characterized radiometric parameters and measurements. For each radiometric cycle of 90 seconds, acquisition is made at seconds: 20, 40, 70, 80 and 90. The acquired data will be interpolated and will lead to a correction factor determined during flight. The top side of the shutter (Sun side) is covered with reflective tape and the bottom side is covered with a vacuum deposition of gold. Table 3 summarizes the main characteristics of SOVAP shutter.

Table 3. SOVAP shutters (right and left) main characteristics.

Shutter diameter	17 mm
Front aperture diameter	13 mm
Opening time	<25 milliseconds
Exposure time	90 seconds

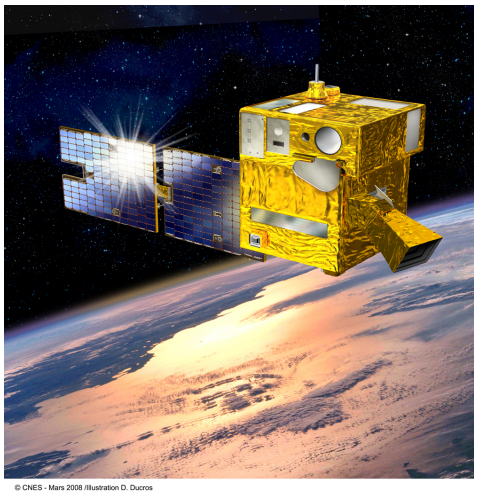

Figure 4. View of the Satellite disposition, SOVAP instrument is at the center.

4. SOVAP ON THE PICARD SATELLITE

The mission took the name of the French astronomer Jean PICARD (1620-1682), who measured the solar diameter, observed the sunspots and determined the Sun rotation velocity. The PICARD payload (Figure 4) is composed of the following instruments: SOVAP, PREMOS (PREcision MOnitor Sensor), and SODISM (SOlar Diameter Imager and Surface Mapper) [12].

5. THE SOVAP MODELS

Models were needed to test the design of the instrument.

5.1 The mechanical analysis

The mechanical design is analyzed with a detailed mathematical model in order to verify stiffness requirements, general and local strength, to be conform to quasi statics loads, random loads but also to establish a stability budget of the optical path. It is a very complex model that requires some verification criteria. The instrument first eigen mode (given by the Finite Element Model) is found equal to 197 Hz which is greater than a given specification of 150 Hz. This is a mechanical improvement compared to the family of DIARAD instruments.

5.2 The thermal analysis

SOVAP has a very high level of thermal symmetry to optimize the accuracy on the TSI. To insure the differential mode of operation of the detectors, we specified a maximum temperature difference between the left and right side of the heat flux sensor better than 0.1^oC. For this, a good thermal contact between the different parts of the structure is guaranteed by design and aimed to reduce the thermal gradients in each panel. A thermal mathematical model was developed to study temperature level variations and thermal gradients affecting the instrument in the two typical cases in orbit and in one stay alive case. The Geometrical Mathematical Model (GMM) is given in Figure 5. The thermal mathematical model has 2306 nodes (428 nodes for SOVAP). CNRS and RMIB have developed a payload model for all the instruments. An optimization of temperature and stability

conditions will be studied in orbit during the commissioning phase. The Temperature Reference Point (TRP) of the instrument is near the interface with the satellite platform. We have however, provided preliminary results obtained from the thermal model (TRP SOVAP between 29.5^{o}C and 32.5^{o}C). The temperatures of the instrument are very stable during the hot case (without eclipse, in June) and during the equinox (March and September). The temperatures of the instrument SOVAP for each case analysis are given in the Figure 6. The switch on temperature of the instrument is -30^{o}C after stay alive case. The switch on temperature of the instrument is -5^{o}C during equinox and when the satellite is pointing the Sun.

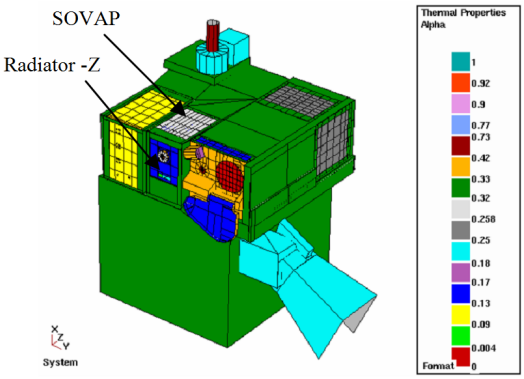

Figure 5. Geometrical Mathematical Model.

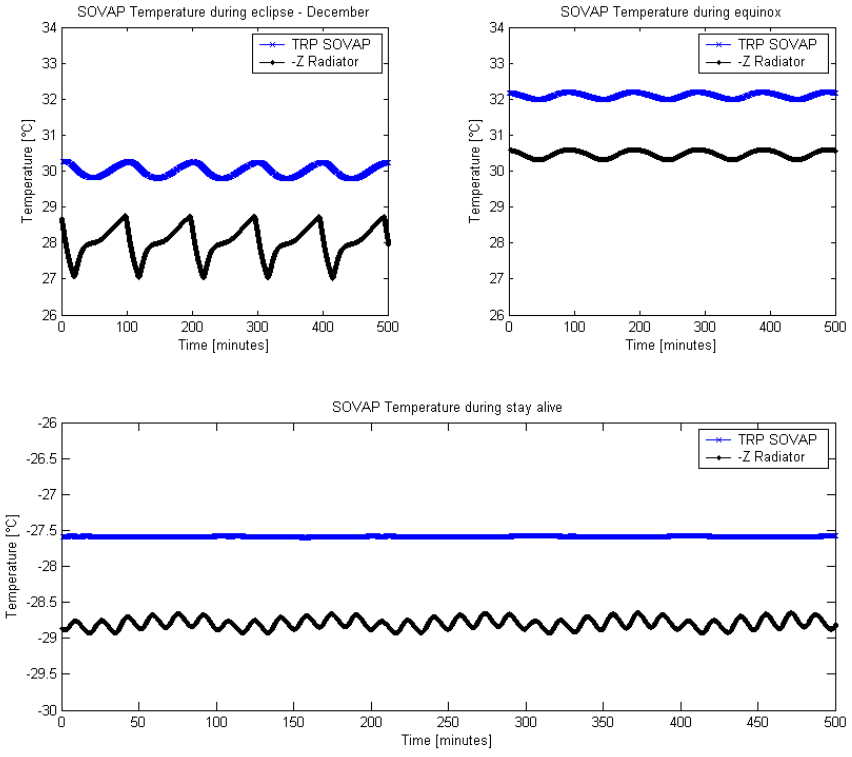

Figure 6. SOVAP temperatures.

5.3 The thermal model of DIARAD

A thermal mathematical model was developed to study temperatures level variations and thermal gradients affecting DIARAD. CNRS and RMIB have developed a DIARAD model. The thermal control was designed using dedicated software (ESARAD and ESATAN from Alstom). Results obtained from the thermal model are given in Table 4 and Figure 7 (for a thermal case, during a special date).

Table 4. Temperatures results obtained by analysis (steady state).

DIARAD element	Temperature [^{o}C]	Gradient in element [^{o}C]
Right Shutter close	30	0.01
Right precision aperture	30.4	0.2
Right heat flux sensor	30.3	0.02
Right cavity tube	30.2	0.02
Left Shutter open	28.5	0.01
Left precision aperture	30	0.02
Left heat flux sensor	30.3	0.02
Left cavity tube	30.2	0.02
Heat sink	30.1	0.02

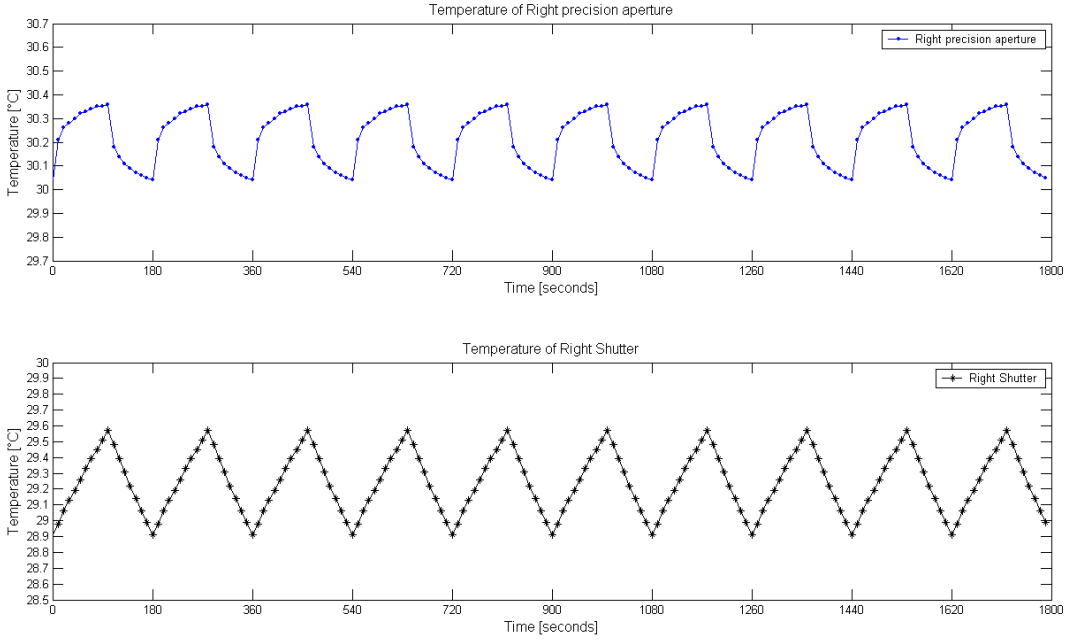

Figure 7. Transient temperature of the most important element of DIARAD.

6. TESTS AND RESULTS FOR QUALIFICATION AND ACCEPTANCE

The environment for the qualification and acceptance tests of the DIARAD/SOVAP instrument are based on: ARIANE sine, DNEPR random, shock (Solar array release with pyrosofts nuts and separation of the micro-satellite with pyro devices), and thermal environment of SSO at 735 km (period of 99.4 minutes). The qualification of the instrument SOVAP was accomplished on the MTS satellite (Mechanical and Thermal Structure). Vibration levels measured on the PICARD MTS have been used for the acceptance testing of the flight model instrument. A thermal balance test was accomplished on the flight model satellite.

6.1 Sinus low level

The instrument third eigen mode found with the sine test, is 320 Hz. The other eigen modes are local. The finite element model we have developed is then representative, since it has given 287 Hz (75% of effective mass of the instrument on Y axis) for the third eigen mode.

6.2 Random vibration

A random vibration has been achieved on the SOVAP instrument flight model with the levels given in the Table 5. This test was performed successfully.

Table 5. Mechanical specifications - Frequency vs PSD (Power Spectral Density).

X axis		Y axis		Z axis	
Frequency	PSD	Frequency	PSD	Frequency	PSD
20 Hz	0.010 g^2/Hz	20 Hz	0.007 g^2/Hz	20 Hz	0.007 g^2/Hz
150 Hz	0.010 g^2/Hz	200 Hz	0.150 g^2/Hz	400 Hz	0.100 g^2/Hz
250 Hz	0.800 g^2/Hz	349.7 Hz	0.150 g^2/Hz	500 Hz	0.300 g^2/Hz
300 Hz	0.800 g^2/Hz	365 Hz	0.010 g^2/Hz	521 Hz	0.300 g^2/Hz
450 Hz	0.100 g^2/Hz	395 Hz	0.010 g^2/Hz	536 Hz	0.010 g^2/Hz
500 Hz	0.100 g^2/Hz	411.6 Hz	0.133 g^2/Hz	566 Hz	0.010 g^2/Hz
550 Hz	0.300 g^2/Hz	700 Hz	0.015 g^2/Hz	581 Hz	0.300 g^2/Hz
600 Hz	0.300 g^2/Hz	1500 Hz	0.015 g^2/Hz	600 Hz	0.300 g^2/Hz
700 Hz	0.007 g^2/Hz	2000 Hz	0.003 g^2/Hz	700 Hz	0.015 g^2/Hz
1500 Hz	0.007 g^2/Hz	–	–	1500 Hz	0.015 g^2/Hz
2000 Hz	0.002 g^2/Hz	–	–	2000 Hz	0.002 g^2/Hz
60 seconds	12.4 g_{rms}	60 seconds	8.18 g_{rms}	60 seconds	8.88 g_{rms}

6.3 Shock test

A shock test was achieved on the MTS satellite for a solar array release with pyrotechnic nuts and separation of the micro-satellite with pyrotechnic devices. This test allowed to qualify the SOVAP instrument.

6.4 Thermal cycling

During the thermal cycling, the instrument was subject to hot and cold environment conditions with temperatures between +50^{o}C and -40^{o}C for non operational conditions. For operational conditions, the instrument thermal cycling was between +45^{o}C and -35^{o}C. This test was performed successfully.

6.5 Thermal balance

A thermal balance test was also achieved with the flight model placed on the PICARD satellite. The results presented in Table 6, show that the instrument behavior is very close to the predictions given by the models.

Table 6. Temperatures results obtains by analysis and tests.

Nominal Case - Instrument ON	Thermal model predictions	Results of the test
TRP SOVAP	25.6^{o}C	23.6^{o}C
Radiator -Z	21.7^{o}C	21.5^{o}C < T < 21.6^{o}C
Stay alive Case - Instrument OFF	Thermal model predictions	Results of the test
TRP SOVAP	-27.9^{o}C < T < -27.8^{o}C	-26.9^{o}C < T < -26.7^{o}C
Radiator -Z	-29.9^{o}C < T < -26.9^{o}C	-28.4^{o}C < T < -27.6^{o}C

7. THE SOVAP INSTRUMENT PERFORMANCES

To derive the most accurate TSI measurements, it is important to understand the error sources of the measuring instrument in order to apply appropriate corrections and to quantify the remaining uncertainties for the temperature and the electrical power measurements. These corrections are used to deliver the final scientific TSI value. Any understanding or neglecting of an error source could lead to a trend or even a discontinuity in the TSI time series. Long-term measurement of the TSI variations is challenging because the order of magnitude of the solar variations, 0.1 % amplitude over an 11 year solar cycle, is close to the absolute accuracy (which is of the order of 1.36 W/m^2) of the radiometers available for measuring these variations. To extract the maximum amount of information about TSI variation it is necessary to minimize the instrumental errors of the available radiometers as much and as objectively as possible. Minimization of the instrumental errors requires a careful instrument design, pre-flight characterization, flight data processing and detailed data analysis including aging corrections. From Earth, the Sun appears as a bright sphere emitting energy over the entire electromagnetic spectrum with wavelengths up to 4 micrometers. The visible part of the Sun or the apparent solar surface is the lower part of a layer called the photosphere. Our focus will be on the solar radiative output and its variability.

7.1 DIARAD/SOVAP description

DIARAD consists of three main parts: the detector, the electrical measurements chains with their references voltages and the servo loop system. DIARAD is used as a heat flux balance with 15 possible radiometric states.

7.1.1 The detectors

The detector is formed by two blackened cylindrical cavities mounted side by side on a common heat sink. Between each cavity and the heat sink, a heat flux sensor and a heating resistor are mounted. Both cavity channels are equipped with a shutter in front to block or admit radiation to the cavity through a precision limiting aperture. Finally an optical baffle separates both channels from the shutters. It is imperative that the whole system be insulated (Multi Layer Insulation or MLI) from the surrounding and as symmetric as feasible.

7.1.2 The servo loop

A description of the detailed feedback loop blocs is given in the Figure 8.

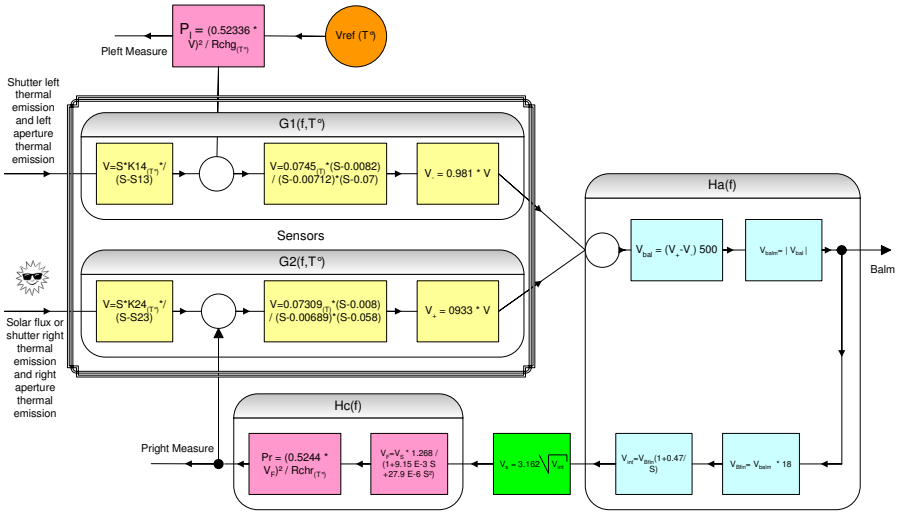

Figure 8. Detailed feedback loop blocs.

Equilibrium between the two trimmed cavities is maintained by an electrical power regulator using an analog Proportional-Integrator feed back loop. DIARAD is mainly operated with the electrical feedback in the irradiated cavity. Although DIARAD may be operated in 15 different radiometric states allowing in-flight determination of some parameters, we will focus the analysis on the two most used modes of operation called active left (radiometric mode A02) and active right (radiometric mode A03). The blocs are detailed hereafter to show what are each peculiar contribution to the final accuracy. Considering Equations 2, 3 and 4, the correction for the static error of servo loop is given by:

$$C_2 = \lim_{f \to 0} \left(\frac{(R_1 + R_m)^2}{R_1 G_1(f,T) H_a(f) H_c(f,T)^2} \right) \tag{1}$$

where R_1 is the heating resistance in the cavity (120 Ohm), R_m is the measurement resistance (100 Ohm), $G_1(f,T)$ is the transfer function of the heat flux sensor (Volt^2/Watt), $H_a(f)$ is the error amplifier gain (Volt^2/ Volt^2), $H_c(f,T)$ is the feed back power gain (Watt/Volt), f is the frequency (Hz) and T is the Temperature (Kelvin).

7.1.3 The electrical chains

Each heating resistor is mounted in series with a current measuring resistor (R_m). The voltage over the four resistors is digitized through four electrical measurement chains. Each electrical chain is composed of a differential amplifier, a voltage to frequency converter and a counter. For the calibration of these electrical chains, DIARAD radiometer use highly accurate reference voltage feeding two precision resistors ladders defining a pair of six potentials. This allows independent in-flight measurement of the function that relates digital count to voltage. The channels 5 and 6 dedicated to the housekeeping acquisition may also be calibrated but not the chains 7 and 8, dedicated to permanent sampling on the BOS.

7.2 Functional description of the radiometers

During the first step (90 seconds) both shutters are closed. A reference power P_{ref} (163 mW) is dissipated in the heating resistor of the passive reference cavity (left) according to: $P_{ref} = V^*I$ where V is the voltage across the heating resistor and I is the current derived from a voltage measurement across a precision resistor. A heat flux is detected by the left heat flux sensor. As a consequence, the servo loop system dissipates a power $P_{cl,r}$ (163 mW) in the measuring or active cavity (right) through its heating resistor. The servo system brings the heat flux sensors G_1 and G_2 outputs V_+ equal to V_- so that $P_{cl,r}$ is at equilibrium with P_{ref} (R06) if $G_1(f,T)$ equals $G_2(f,T)$. During the second step (90 seconds) only the active shutter opens. For a perfectly black cavity, without any thermal loss, an absorbed Solar power SI^*A_r is detected by the heat flux sensor where SI is the Solar Irradiance (1366 W/m^2 for example) and A_r the surface of the right precision aperture (square meter). As a consequence, the servo loop system dissipates a power $P_{o,r}$ (59 mW) in the measuring cavity (right) through its heating resistor. In this case, the Sun brings 104 mW to the flux sensor. DIARAD provides thus every three minutes a measurement of the solar irradiance.

7.3 Absolute accuracy

The TSI is defined as the solar irradiance at the mean Earth-Sun distance according to:

$$TSI = SI \frac{r^2}{(1A.U.)^2} \frac{1}{(1 - \frac{\partial r}{\partial t}\frac{1}{c})^2} \tag{2}$$

where TSI is the Total Solar Irradiance in W/m^2 at 1 A.U., SI is the Solar Irradiance in W/m^2, r is the distance between the satellite and the Sun in km, $1A.U.$ is 1 Astronomical Unit (149,597,870.691 km), c is the speed of light (299792.458 km per second) and t is the time in second.
SI is derived from the measurement of the electrical power supplied to the active cavity (right for example SI_r) of the radiometer to maintain the active cavity with the same heat sink flux in the open and closed states (Equation 3) according to:

$$SI_r = C_5 \frac{(\overline{(P_{cl,r}} - P_{o,r}) + C_1 + C_6)(1 - C_2)}{\alpha_{eff,r} A_r (1 + \Delta_r + \Delta'_r + \Delta''_r) \cos\theta} + C_3 + C_4 \tag{3}$$

$$\overline{P_{cl,r}} = \frac{P_{cl,r,t1} + P_{cl,r,t3}}{2} \tag{4}$$

where SI_r is the Solar Irradiance for the right cavity of the radiometer, C_5 (see Equation 5) is the total correction factor for the optical effects (the diffraction, the scattering around the 2 apertures in front of the cavity and the backscattered radiation from the volume between the shutter and the precision aperture), $P_{cl,r,t1}$ is the electrical power (W) fed to the right cavity in closed state of the shutter at the time t1, $P_{cl,r,t3}$ is the electrical power (W) fed to the right cavity in closed state of the shutter at the time t3, $P_{o,r}$ is the electrical power (W) fed to the right cavity in open state of the shutter at the time t2, C_1 is the correction to take into account the wires heating effect, C_2 is the correction for the accuracy of the servo-system (almost negligible) and monitored with Balm (see Figure 8), $\alpha_{eff,r}$ is the efficiency of the right cavity, A_r is the measured accurate area of the aperture at $+20^o$C, Δ_r is the correction factor of the area of the aperture generated by the thermal effect on the aperture (dilatation), Δ'_r is the correction factor of the area of the aperture generated by thermo-mechanical effect of the instrument, Δ''_r is the correction factor of the area due to the mechanical constraints induced by the fixture of the precision apertures in their supports, θ is the solar pointing angle of the instrument, C_3 is the right shutter emission correction function based on its temperature emissivity and view factor to A_r, C_4 is the right mirror emission correction function based on its temperature emissivity and view factor to A_r and C_6 is the dynamic non equivalence of the sensors to take into account the equations: $G_1(f,T) \neq G_2(f,T)$, and depends of the the mode of operation of the radiometer. Equation 3 is of course valid if the radiometer has been adjusted to provide zero at the difference of the thermoelectric detectors, i) when the electric power is applied to both cavities, ii) when the detector amplifier read zero when both shutter are closed and the radiometer is in thermal equilibrium.

We have two cavities in DIARAD/SOVAP. All the commentaries given for the right cavity are applicable for the left cavity. The SOVAP instrument performances are detailed hereafter: $a-$ Uncertainty associated to the detectors: $\alpha_{eff,r}$, A_r, Δ_r, Δ'_r, Δ''_r, C_5, $\cos\theta$, including thermo-mechanical sliding of the instrument, C_3 and C_4. $b-$ Uncertainty associated to the electronics: accuracy of the feed back loop C_2, sensors ($G_1(f,T)$ and $G_2(f,T)$) thermal equilibrium error C_6, and measurements of the parasite heating resistors C_1. $c-$ Uncertainty associated to the electrical acquisition chains value and stability of the voltage references, noise levels of the acquisition chains, accuracy of the current measurements resistors and knowledge of the heating resistors in function of the temperature.

7.3.1 Precision Aperture A_r

The area should be chosen as large as possible in order to be able to measure it with a high relative accuracy. The precision apertures have been measured at JPL, NIST and NPL at $+20^o$C with 1S to the left and 2S to the right (Figure 9). As NPL and NIST are state of the art institutions, we do not decide which results are best and we use the mean of those results, which has a very negative impact on the uncertainty budget. Although each result could be properly balanced by its standard deviation to grant the most repeatable method. We have 214 ppm (k=2) uncertainty for the left aperture and 234 ppm (k=2) uncertainty for the right aperture on the measurements. The instrument use Titanium precision apertures. Precision Aperture A_r at 20^oC is equal to 7.875925 10^{-5} m^2.

7.3.2 Correction factor of the area of the aperture

Knowledge of the precision area aperture is fundamental for determining the value of the TSI (Table 7). The deformation of the aperture is due at three cases: the dilatation of the mirror and the deformation of the instrument (about 30^oC).

Table 7. Thermo-mechanical effects on the precision aperture.

Element Radius	[mm]	Area [mm^2]	Delta [mm^2]
Reference Aperture at 20^oC	5.000	78.540	–
Aperture at 30^oC	5.0005	78.556	0.016
Deformation Aperture at 30^oC	5.003	78.634	0.094

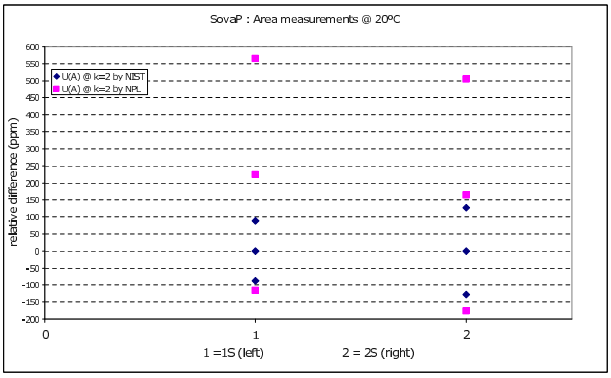

Figure 9. Measurements on the precision aperture.

Correction factor Δ_r of the area of the aperture

We have for both the left and right cavity a parameter of correction for the area A_r due to the thermal dilatation of the precision aperture at $+30^o$C. Δ_r is estimated at 0.000172 at $+30^o$C for the right cavity (or 0.235 W/m^2). The uncertainty on this thermal correction is 30 ppm or 0.041 W/m^2.

Correction factor Δ'_r of the area of the aperture

We have for both the left and right cavity a parameter of correction for A_r due to the thermo-mechanical effect of the instrument. Δ'_r is estimated at 0.00119 for the right cavity. The uncertainty on this thermal correction is 250 ppm or 0.341 W/m^2. It is important to understand and to measure Δ'_r with an appropriate test.

Correction factor Δ''_r of the area of the aperture

When we clamp the mirror, we have a deformation of the area of the aperture. Δ''_r is estimated at 0 for the right cavity. The uncertainty on this correction is 250 ppm or 0.341 W/m^2. It is important to understand and to measure Δ''_r with an appropriate test. The deformation of the precision aperture is shown in Figure 10.

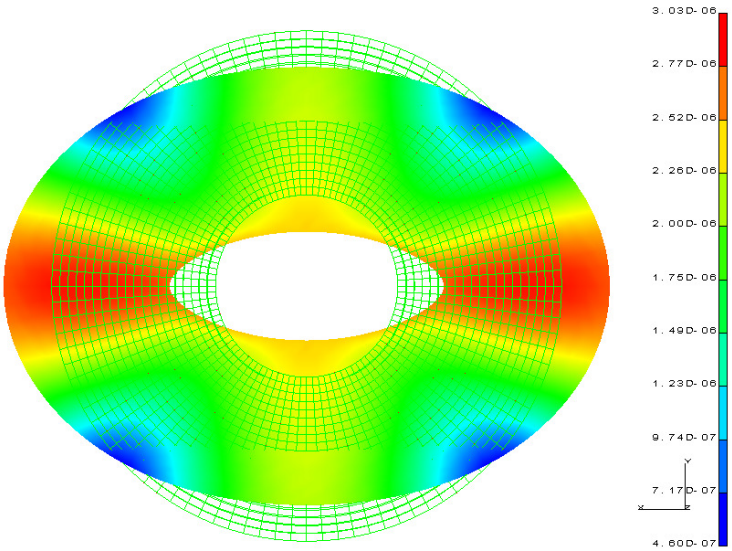

Figure 10. Deformation of the precision aperture (in meter).

7.3.3 Absorption factor of the cavity $\alpha_{eff,r}$

Solar absorptance of the cavity (black paint) is between 0.92 and 1. The absorption factor of the cavity is calculated with the thermal model of the cavity. The results are given in Figure 11.

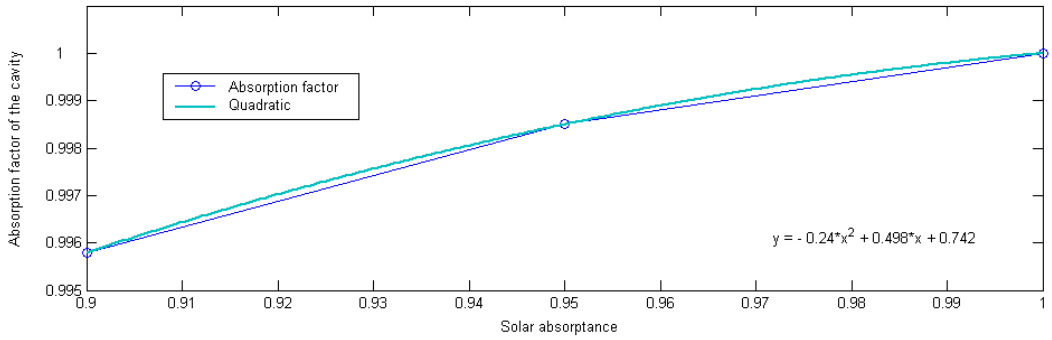

Figure 11. Absorption factor of the cavity.

The solar absorptance (Nextel black velvet) used on DIARAD is of the order of 0.96. Absorption factor of the cavity has been calculated with the thermal model (including the thermoelectric detector clamped on the heat sink) and we obtain a factor of 0.998896 for $\alpha_{eff,r}$. We have a parameter of correction from unitary absorption of +1.507 W/m^2. From knowledge of the solar absorptance with an uncertainty of $\pm 0.5\%$, the absorption factor of the cavity gives an uncertainty of ± 0.259 W/m^2 or ± 190 ppm.

7.3.4 Total correction factor for the optical effects C_5

These effects are: the diffraction, the scattering around the 2 apertures in front of the cavity and the backscattered radiation from the volume between the shutter and the precision aperture. The experimental determination of the diffraction and scattering errors around the apertures is difficult because these effects are relatively small (Crommelynck, 1982). It is given by the Equation:

$$C_5 = \frac{1}{\Sigma + \Sigma' + \delta} \tag{5}$$

where, Σ is the backscattered radiation, Σ' the scattering around the aperture in front of the cavity and δ is the diffraction. The design is similar with DIARAD/VIRGO. We can take the same value by analogy. We have $\Sigma = 0.75 * 10^{-5}$. This value is estimated from SOLCON characterization. We have $\Sigma' = 4.5 * 10^{-5}$. This value is estimated from SOLCON characterization. δ is the order of $5 * 10^{-4}$. That is a NIST estimated value. We have a parameter of correction of +0.754 W/m^2. From the knowledge of this parameter with an uncertainty of $\pm 20\%$, the total correction factor for the optical effects gives an uncertainty of ± 0.150 W/m^2 or ± 110 ppm. A description of the fraction of additional solar flux stray-light is given in the Figure 12.

7.3.5 Solar pointing angle with the instrument θ

The satellite is stabilized by a two-level optical system, i) stars are used to achieve a pre-pointing within a few degrees, ii) a four-quadrant system of SODISM [12] achieves a pointing within 36 arc seconds. Given the good pointing of PICARD, this effect is negligible. The alignment between SOVAP and SODISM was measured on ground.

7.3.6 Thermo-mechanical sliding of the instrument $\cos\theta$

Between the nominal case (solar pointing) and the stay alive case, the line of sight of the instrument SOVAP can move a maximum of 12 arc minutes and randomly. The total uncertainty on this parameter is ± 0.008 W/m^2 or ± 6 ppm.

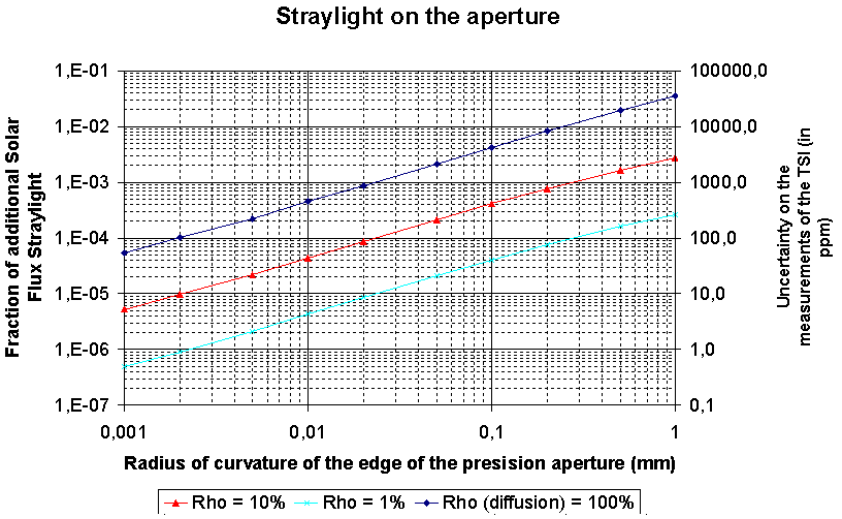

Figure 12. Stray-light on the precision aperture.

7.3.7 Internal infrared emission of the shutter C_3

This correction takes into account the contribution of the internal thermal emission of the active shutter. This contribution is removed when the shutter is open. The left cavity is closed and the sensor sees the left shutter. The right cavity is open and the sensor sees deep space. For DIARAD the shutter correction is determined during deep space pointing just after the solar period (during 20 minutes). During this phase, the temperature of the shutter change significantly. It's necessary to make a model and to verify it during the operational phase. It is given by the Equations:

$$Q_{s-shutter} = \frac{1}{\frac{1-\varepsilon_s}{\varepsilon_s} + \frac{1}{F_{s-shutter}} + \frac{1-\varepsilon_{shutter}}{\varepsilon_{shutter}} \frac{S_s}{S_{shutter}}} S_s \sigma (T_s^4 - T_{shutter}^4) \tag{6}$$

$$F_{s-shutter} = \frac{1}{2} X'' - \frac{1}{2} \sqrt{X''^2 - 4 \frac{r_{shutter}^2}{r_s^2}} \tag{7}$$

$$X'' = 1 + \frac{1 + \frac{r_{shutter}^2}{h_s^2}}{\frac{r_s^2}{h_s^2}} \tag{8}$$

where, $Q_{s-shutter}$ is the power exchange between the sensor and the shutter (W), ε_s is the emissivity of the sensor, $\varepsilon_{shutter}$ is the emissivity of the shutter (back face), S_s is the area of the sensor (m^2), $F_{s-shutter}$ is the view factor between the sensor and the shutter, $S_{shutter}$ is the area of the shutter (m^2), σ is the Stefan-Boltzmann constant (5.6704 10^{-8} $W/m^2/K^4$), T_s is the temperature (Kelvin) of the sensor, $T_{shutter}$ is the temperature (Kelvin) of the shutter, $r_{shutter}$ is the radius (m) of the shutter, r_s is the radius (m) of the sensor, h_s is the distance (m) between the sensor and the shutter and X'' is a constant. We have a parameter of correction of -1.06 W/m^2. It is possible to make a calibration on deep space during the mission. This measurement will be very important. The total uncertainty on this parameter is ± 0.053 W/m^2 or ± 39 ppm.

7.3.8 Internal infrared emission of the mirror C_4

This correction takes into account the contribution of the internal thermal emission of the mirror (aperture). When the right cavity is open, the solar flux heats the right mirror. It is given by the Equations:

$$Q_{s-m} = \frac{1}{\frac{1-\varepsilon_s}{\varepsilon_s} + \frac{1}{F_{s-m}} + \frac{1-\varepsilon_m}{\varepsilon_m}\frac{S_s}{S_m}} S_s \sigma (T_s^4 - T_m^4) \tag{9}$$

$$F_{s-m} = \frac{1}{2}X - \frac{1}{2}\sqrt{X^2 - 4} - \frac{1}{2}X' + \frac{1}{2}\sqrt{X'^2 - 4\frac{r_{m-int}^2}{r_s^2}} \tag{10}$$

$$X = 1 + \frac{1 + \frac{r_{m-ext}^2}{h^2}}{\frac{r_s^2}{h^2}}, \qquad X' = 1 + \frac{1 + \frac{r_{m-int}^2}{h^2}}{\frac{r_s^2}{h^2}} \tag{11}$$

where, Q_{s-m} is the power exchange between the sensor and the mirror (W), ε_s is the emissivity of the sensor, ε_m is the emissivity of the mirror (back face), S_s is the area (m^2) of the sensor, F_{s-m} is the view factor between the sensor and the mirror, S_m is the area (m^2) of the mirror, σ is the Stefan-Boltzmann constant, T_s is the temperature (Kelvin) of the sensor, T_m is the temperature (Kelvin) of the mirror, r_{m-int} is the internal radius (m) of the mirror exposed to the solar radiation, r_{m-ext} is the external radius (m) of the mirror, r_s is the radius (m) of the sensor, h is the distance (m) between the sensor and the mirror, X is a constant and X' is a constant. We have a parameter of correction of +0.13 W/m^2. The total uncertainty on this parameter is ±0.026 W/m^2 or ±19 ppm.

7.3.9 Precision of the servo-system C_2

The static or position error of the feedback loop is equal to 0. The total uncertainty on this parameter is ±1.2 ppm.

7.3.10 Dynamic non equivalence C_6 and internal infrared emission of the tube

C_6 correction factor must be introduced due to the non thermal equilibrium of the Peltier elements ($G_1(f,T)$ and $G_2(f,T)$). This effect is essentially a differential error of the DIARAD detector, usage of the different radiometric states allows through the measurements of Balm (see Figure 8) to find the correction for this C_6 error. The time response of the servo-system for the right cavity is near 1 second at 1σ. The time response of the servo-system for the left cavity is near 1.2 second at 1σ. But the difference of thermal field in the irradiated detector and the occulted detector introduce a passive thermal response depending of the temperature of the detector box and the temperature of the tube (see Figure 13). The total uncertainty on this parameter is ±0.018 W/m^2 or ±13 ppm for a difference of temperature of ±0.001^{o}C in the cavity.

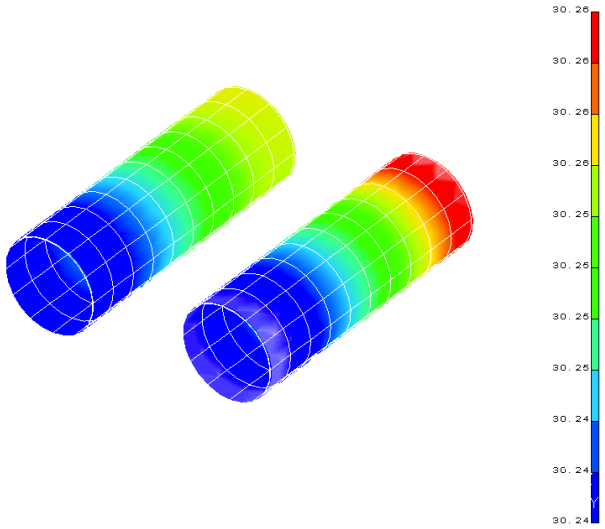

Figure 13. Temperatures in the occulted detector tube and in the irradiated detector tube [^{o}C].

7.3.11 Uncertainty associated to the electrical chains

During the receipt of the instrument we noticed that each channel has different characteristics and that the fourth channel has an abnormal behavior. Due to the very tight schedule it was decided to accept this loss of performance. This has for consequence that all the data acquired by channel 4 will be affected (right voltage and the temperature of the converters). For the left cavity the classical power calculation by the voltage product of the current leads to an uncertainty of ±294 ppm or ±0.4 W/m^2. For the right cavity, we must introduce a model for the thermal behavior of the right heating resistor obtained during the thermal vacuum test.

$$P_r = R_1 \frac{U_m^2}{R_m^2(T)} \tag{12}$$

where P_r is the power (W) in the right heater and U_m is the measurement voltage across the resistance R_m at temperature T. The uncertainty for the right cavity is ±518 ppm or ±0.7 W/m^2. We must introduce a correction for the transfer of calibration due to the difference of source impedance. We need also to take into account a correction for a parasitic resistance introduced during the repair of the flight model.

7.4 Resolution

The comparison of DIARAD/VIRGO and TIM/SORCE or DIARAD SOVIM, has demonstrated that each instrument has a repeatability of 0.1 W/m^2. SOVAP has the same heritage than VIRGO. The resolution will be better than 0.01 W/m^2.

7.5 Absolute accuracy synthesis

Uncertainty for the absolute accuracy (right and left cavity) is given in table 8. TSI uncertainty from DIARAD/SOVAP will be less than ±2.77 W/m^2 (Total with adjustment) for the right channel and ±2.27 W/m^2 (Total) for the left channel.

Table 8. Uncertainty on the measurements of the TSI.

Cavity	Right		Left	
Parameters	[ppm]	[W/m^2]	[ppm]	[W/m^2]
Precision Aperture A_r	117	0.160	107	0.146
Thermal effects Δ_r	30	0.041	30	0.041
Thermo-mechanical effect Δ'_r	250	0.341	250	0.341
Fixation of the aperture Δ''_r	250	0.341	250	0.341
Absorption factor $\alpha_{eff,r}$	190	0.259	190	0.259
Optical effects C_5	110	0.150	110	0.150
Solar pointing angle $\cos\theta$	0	0.000	0	0.000
Thermo-mechanical sliding $\cos\theta$	6	0.008	6	0.008
Infrared emission of the shutter C_3	39	0.053	39	0.053
Infrared emission of the mirror C_4	19	0.026	19	0.026
Infrared emission of the tube	13	0.018	13	0.018
Accuracy of the servo-system C_2	1.2	0.002	1.2	0.002
Sensor thermal equilibrium error C_6 at 90 seconds	162	0.221	214	0.293
Wire heating effect C_1	1.5	0.002	0.8	0.001
Electrical chains (general effects)	518	0.707	294	0.401
Electrical chains (transfer of calibration)	124	0.169	121	0.165
Electrical chains (ground parasitic resistance)	201	0.270	20	0.027
Total uncertainty (1σ)	2032	2.77	1665	2.27
Mean quadratic uncertainty (1σ)	735	1.00	579	0.79

7.6 Parameters measurements for the Total Solar Irradiance

The parameters for the measurement of the Solar Irradiance (used in Equation 3) are defined in Table 9. TSI is defined as the amount of radiant energy emitted by the Sun over all wavelengths and outside Earth's atmosphere. The TSI is defined as the solar irradiance at the mean Earth-Sun distance according to the Equation 2.

Table 9. Instrument parameters measurements.

Parameters	Value	Remarks
$\overline{P_{cl,r}} - P_{o,r}$	0.104 W	To be confirmed during operation phase
C_1	5.9 10^{-6} W	To be confirmed during operation phase
C_2	1.2 10^{-6}	
C_3	-1.06 W/m^2	To be confirmed during operation phase
C_4	+0.13 W/m^2	To be confirmed during operation phase
C_5	0.999447805	
C_6 at 90 seconds	16.8 10^{-6} W	To be confirmed during operation phase
$\alpha_{eff,r}$	0.998896	
A_r at 20^{o}C	7.875925 10^{-5} m^2	
Δ_r	0.000172	To be confirmed during operation phase
Δ'_r	0.00119	To be confirmed during operation phase
Δ''_r	0	To be confirmed during operation phase
$\cos\theta$	1	

8. CONCLUSION

The TSI (Total Solar Irradiance), and helioseismologic oscillations, the solar diameter, the limb shape and the solar asphericity, are key parameters for characterizing the physics of the Sun. They constitute fundamental quantities to validate the Sun modeling, i. e. the functioning of our star. To achieve these key measurements, radiometers are used to measure the TSI. The final performances of the SOVAP instrument will be acquired during the first year of the return of the data (adjustment of major parameters). The instrument has been characterized in detail, and space qualified. Concerning the future acquired data, the TSI value from DIARAD/SOVAP will be of the order of 1366.0 W/m^2 (To be confirmed during flight). The mean quadratic uncertainty of the left cavity is $\pm$0.79 W/m^2 and $\pm$1.00 W/m^2 for the right cavity. This uncertainty manifest a slight deviation from the scientific requirements (having an absolute accuracy better than $\pm$1.36 W/m^2). The nominal cavity for the flight is the right cavity. The precision will be better than 0.1 W/m^2 and with a resolution better than 0.01 W/m^2. For the adjustment of the measurements, we need to characterize the correction factor of the fixation of the mirror, the correction factor of the area of the aperture, the absorption factor of the cavity and the thermal time constants of the detectors, afterward, it is feasible to plenty fulfill the scientific requirements. The scientific payload composed of SODISM, PREMOS and SOVAP benefits of data exchange between the different instruments. Since the launch, we have noticed, that due to a contamination, the mean temperature of the instrument is above the model predicted temperature (roughly 10^{o}C). Due to this rise of temperature, we have experienced an eventual failure of the right shutter. Due to this failure, we have been driven to use the radiometer in different radiometric modes than the nominal foreseen mode (A02 and A03). The uncertainty budget presented here does not represent the budget error in all the in-flight modes of operation because it does not take account a specific model of the calibration voltage in each mode nor the difference of time response of the detector when they are or not included in the feed back loop. Presently, the nominal mode of operation is a classic radiometric but not nominal (R10) with a monthly contingency right shutter open failure mode (A08). The data treatment was not foreseen to take into account those kind of operations. The uncertainty budget can be reduced at the conditions: to obtain traceable measurement of the paint used in the cavity to calculate $\alpha_{eff,r}$, to adjust correction C_6 (thermal emissivity of the tubes and thermal contact of the tubes and the detector), to determine the deformation of the precision aperture Δ'_r and Δ''_r, and to take into account the systematic electrical change calibration error. The SOVAP radiometer has been in orbit for one year and is operational.

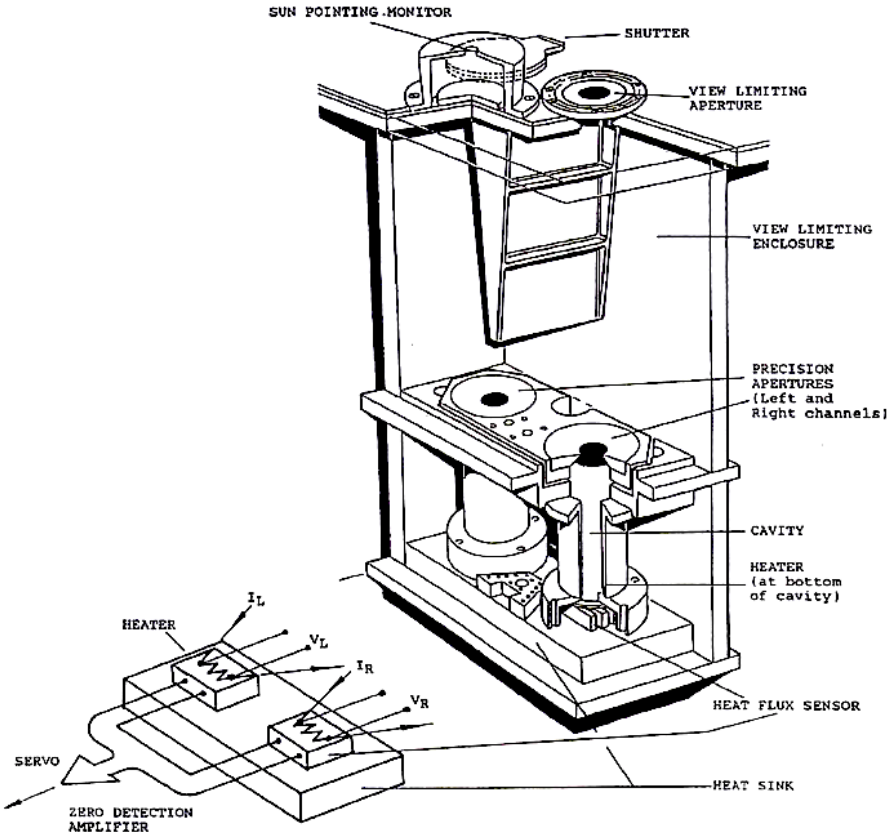

Figure 14. DIARAD/SOVAP cavity principle.

ACKNOWLEDGMENTS

The SOVAP instrument has been built by RMIB and CNRS. We thank RMIB, CNRS LATMOS (Laboratoire, ATmosphere, Milieux, Observations Spatiales) ex Service d'Aéronomie and CNES (Centre National d'Etudes Spatiales) for their support. We thank our collaborators for the design and fabrication of the instrument, including the important help of Pierre Malcorps, Sami Bali and Joël Pierard.

REFERENCES

1. G. Thuillier, S. Sofia, M. Haberreiter and the PICARD team, Past, Present and Future Measurements of the Solar Diameter, Adv. Space Res. 35, 329-340, 2005.
2. G. Thuillier, S. Dewitte, W. Schmutz and the PICARD team, Simultaneous Measurements of the Total Solar Irradiance and Solar Diameter by the PICARD mission, Adv. Space Res., 1792-1806, 2006.
3. D. Crommelynck, Fundamentals of absolute pyrheliometry and objective characterizations, In J.B. Hall, Jr Editor, NASA Earth Radiation Science Seminar, pp. 53-88, August 1982.
4. Fröhlich C., Romero J., Roth H., Wehrli C., Andersen B.N., Appourchaux T., Domingo,V., Telljohann,U., Berthomieux, B., Delache P., Provost J., Toutain T., Crommelynck D., Chevalier A., Fichot A., Dappen W., Gough D., Hoeksema T., Jimenez A., Gomez M. F., Herreros J. M., Roca Cortes T., Jones A. R., Pap J. M., Willson R. C., VIRGO: Experiment for Helioseismology and Solar Irradiance Monitoring, Solar Phys., Volume 162, Issue 1-2, pp. 101-128, 1995.
5. D. Crommelynck, in N Fox (Ed.) New Developments and Applications in Optical Radiometry, Inst. Phys. Conf. Ser. 92, London, p19, 1988.
6. NPL Certificate of calibration LD07/00021/C21/1 (14 November 2000).

7. Carol Johnson B., Litorja M., Fowler J., Crommelynck D., Dewitte S., Fröhlich C., Lee R.B. III, Willson R.C., Helizon R., Barnes R., Butler J.J., NIST Results of aperture area comparisons for exo-atmospheric total solar irradiance measurements.
8. S. Mekaoui, S. Dewitte, Total Solar Irradiance Measurements and modeling during cycle 23, Solar Physics, Volume 247, Issue 1, pp. 203-216, 2008.
9. D. Crommelynck, V. Domingo, Solar irradiance observations, Science 225, 180-181, 1984.
10. Dewitte, S., Crommelynck, D., Joukoff, A., Total Solar Irradiance observations from DIARAD/VIRGO, Journal of Geophysical Research, Volume 109, Issue A2, CiteID A02102, 2004.
11. Dewitte S., Joukoff A., Crommelynck D., Lee III R.B., Helizon R., Wilson R.S, Contribution of the SOLCON program to the long term total solar irradiance observation, Journal of Geophysical Research, Volume 106, Issue A8, p. 15759-15766, 2001.
12. M. Meftah, M. Meissonnier, A. Irbah, S. Abbaki, P. Assus, E. Bertran, J.P. Dubois, E. Ducourt, C. Dufour, J.P. Marcovici, G. Poiet, A.J. Vieau, G. Thuillier, The Space instrument SODISM and the Ground instrument SODISM II, SPIE, Volume 7731, pp. 773145-773145-12, 2010.
13. Eric L. Shirley, Diffraction corrections in radiometry: spectral and total power and asymptotic properties, Vol. 21, No. 10/October 2004/J. Opt. Soc. Am. A., 2004.
14. Hickey, J.R.; Stowe, L.L.; Jacobowitz, H.; Pellegrino, P.; Maschhoff, R.H.; House, F.; Vonder Haar, T.H.; Initial Solar Irradiance from NIMBUS 7 Cavity Radiometer Measurements, Science, Volume 208, Issue 4441, pp. 281-283, 1980.
15. Hickey, John R.; Alton, Bradley M.; Kyle, H. Lee; Hoyt, Douglas; Total Solar Irradiance measurements by ERB/NIMBUS-7 - A review of nine years, Space Science Reviews (ISSN 0038-6308), vol. 48, no. 3-4, pp. 321-342, 1988.
16. Kyle, H.L., Hoyt, D.V. & Hickey, J.R., A review of the Nimbus-7 ERB solar dataset, Solar Phys., 152, 9-12, 1994.
17. Willson, R.C. & Hudson, H.S., Solar Maximum Mission experiment - Initial observations by the active cavity radiometer, Advances in Space Research, 1, 285-288, 1981.
18. Willson, R.C., Gulkis, S., Janssen, M., Hudson, H.S. & Chapman, G.A., Observations of solar irradiance variability, Science, 211, 700-702, 1981.
19. Barkstrom, B.R., The Earth Radiation Budget Experiment (ERBE), Bulletin of the American Meteorological Society, 65, 1170-1185, 1984.
20. Lee, R.B., III, Barkstrom, B.R. & Cess, R.D., Characteristics of the earth radiation budget experiment solar monitors, Applied Optics, Vol. 26, Issue 15, pp. 3090-3096, 1987.
21. Barkstrom, B.R., Harrison, E.F. & Lee, R.B., III, Earth Radiation Budget Experiment - Preliminary seasonal results, EOS Transactions, 71, 297, 1990.
22. Willson, R.C. & Mordvinov, A.V., ACRIM2 Observations and the Long Term, Total Solar Irradiance Database, AGU Fall Meeting Abstracts, 2001.
23. Crommelynck, D., Domingo, V. & Fröhlich, C., The Solar Variations (SOVA) experiment in the EURECA space platform, Advances in Space Research, 11, 83-87, 1991.
24. Crommelynck, D., Domingo, V., Fichot, A., Fröhlich, C., Penelle, B., Romero, J. & Wehrli, C., Preliminary Results from the SOVA Experiment on Board the European Retrievable Carrier (EURECA), Metrologia, 30, 375-379, 1993.
25. Romero, J., Wehrli, C. & Fröhlich, C., Solar total irradiance variability from SOVA 2 on board EURECA, Solar Phys., 152, 23-29, 1994.
26. Fröhlich, C., Crommelynck, D., Wehrli, C., Anklin, M., Dewitte, S., Fichot, A., Finsterle, W., Jiménez, A., Chevalier, A. & Roth, H., In-Flight Performance of the Virgo Solar Irradiance Instruments on SOHO, Solar Phys., 175, 267-286, 1997.
27. Finsterle, W., Fröhlich, C. & Schlifkowitz, U., Review of the Long-Term Performance of the PMO6 Radiometers on VIRGO/SOHO, In SOHO-17, 10 Years of SOHO and Beyond, vol. 617 of ESA Special Publication, 2006.
28. Willson, R.C. & Helizon, R.S., EOS/ACRIM III instrumentation, SPIE, vol. 3750, 233-242, 1999.
29. Kopp, G., Lawrence, G. & Rottman, G., The Total Irradiance Monitor (TIM): Science Results, Solar Phys., 230, 129-139, 2005.